Alloying Effects on Surface Stability and Creep Strength of Nickel Based Single Crystal Superalloys containing 12mass%Cr

Y. Murata [1], R. Hashizume [2], A. Yoshinari [3], N. Aoki [1], M. Morinaga [1], and Y. Fukui [3]

1) Department of Materials Science and Engineering, Graduate School of Engineering, Nagoya University, Furo-cho, Chikusa, Nagoya 464-8603, JAPAN,
   TEL & FAX +81 52 789 3232
   E-mail : murata@numse.nagoya-u.ac.jp
2) Materials Research Section, Technical Research Center, The Kansai Electric Power Company Inc., 11-20 Nakoji 3-chome, Amagasaki 661-0974, JAPAN
3) Hitachi Research Laboratory, Hitachi Co. Ltd., 3-1-1 Ohmika, Hitachi, 317-8511, JAPAN

Abstract

A series of experiments is carried out with six nickel based single crystal superalloys for use in industrial gas turbines. Each alloy contains 12mass%Cr, but no Re. The alloy compositions are chosen with the aid of the d-electrons concept, so that any undesirable phases do not appear in the alloy. The creep rupture life is measured at a stress of 196MPa and a temperature of 1193K, which is close to the service temperature, 1150K, of industrial gas turbines in power plants. The measured life of two alloys in this condition is found to be comparable to that of the 2nd generation nickel based single crystal superalloy containing 3%Re alloy. Also, it is shown that the amount of 12mass%Cr is not necessary to get good hot-corrosion resistance, as long as both the compositional ratios of Ti/Al and Ta/(W+Mo) are high in the alloy. In addition, a dense TiO_2-rich layer is found on the surface of the alloy with good hot-corrosion resistance. In contrast to the hot-corrosion resistance, the oxidation resistance is lowered if the Ti/Al compositional ratio is high in the alloy. The possible mechanisms for hot corrosion and oxidation are discussed in this study.

Introduction

The importance of the combined cycle system in power plants has been increasing, because it has a great potential for the increase in the efficiency of power generation and also the attendant decrease in the emission of carbon dioxide into the air [1]. Nickel-based superalloys used for this system should be superior in hot corrosion resistance and oxidation resistance to the conventional alloys used for jet engines. This is because the examination interval for the maintenance of the system is much longer than that of jet engines. Another reason is partially due to the location of the power plant since it is often placed near the seaside, in particular, in Japan. There is a strong attack to the system when exposed to an NaCl corrosive atmosphere.

Furthermore, the nickel based superalloys for jet engines have been developed so as to increase the creep strength at the temperatures of more than 1300K [2,3]. However, the metal temperature of gas turbines is usually below 1170K. In addition, it has been found that the alloys with superior creep strength at high temperatures are not necessarily strong at low temperatures, as shown later. Thus, there are distinct differences in the targets for alloy design between jet engines and gas turbines.

The purpose of this study is to get fundamental information necessary for the design of single crystal superalloys for use in industrial gas turbines. The alloying effects are investigated experimentally on the surface stability and the creep strength of the alloys.

Experimental Procedure

Alloy chemistry

Six nickel-based single crystal superalloys containing 12mass%Cr, NKH71 ~ NKH76, are made with the aid of the

Table 1 Chemical compositions and alloying parameters of experimental alloys (mol%/mass%)

Alloy	Ti	Cr	Co	Nb	Mo	Hf	Ta	W	Al	Ni	$\overline{Md}$	$\overline{Bo}$	Ti/Al	Mo+W	Ta/(Mo+W)
NKH71	1.51	13.99	0.00	0.00	0.30	0.00	1.91	2.52	11.02	bal.	0.985	0.688	0.137	2.82	0.68
	1.21	12.19	0.00	0.00	0.49	0.00	5.78	7.75	4.98						
NKH72	1.57	14.09	3.87	0.00	0.31	0.00	1.91	2.50	10.89	bal.	0.987	0.696	0.144	2.81	0.68
	1.26	12.27	3.81	0.00	0.50	0.00	5.78	7.70	4.92						
NKH73	2.99	14.05	0.00	0.06	0.36	0.01	2.17	1.98	9.01	bal.	0.985	0.694	0.332	2.34	0.93
	2.39	12.20	0.00	0.09	0.57	0.04	6.57	6.09	4.06						
NKH74	4.74	14.13	3.97	0.06	0.36	0.01	2.20	1.96	7.30	bal.	0.995	0.712	0.649	2.31	0.95
	3.77	12.20	3.88	0.09	0.57	0.03	6.61	5.97	3.27						
NKH75	2.98	14.07	3.93	0.06	0.30	0.01	1.99	1.86	8.76	bal.	0.980	0.697	0.340	2.16	0.92
	2.40	12.28	3.89	0.09	0.48	0.03	6.05	5.74	3.97						
NKH76	4.92	14.11	0.00	0.06	0.30	0.01	1.78	1.77	7.48	bal.	0.989	0.698	0.658	2.06	0.86
	3.97	12.36	0.00	0.09	0.48	0.03	5.43	5.47	3.40						
3%Re*	1.27	7.60	9.96	0.00	0.38	0.03	2.19	2.12	12.62	bal.	0.986	0.667	0.101	3.46**	0.88
	1.00	6.50	9.65	0.00	0.60	0.10	6.50	6.40	5.60						

*) 3%Re alloy contains 2.95mass%Re and is used as a reference alloy.   **) Mo+W+Re

Table 2 Heat treatment conditions employed in this study

Alloy	Solution	1st Step aging	2nd Step aging
NKH71	1573K/28.8ks	1373K/14.4ks, A.C.	1144K/72ks, A.C.
NKH72			
NKH73			
NKH74	1553K/14.4ks + 1558K/14.4ks		
NKH75	1573K/28.8ks	1393K/14.4ks, cooling to 1144K at a rate of 0.03K/s	
NKH76	1553K/14.4ks + 1558K/14.4ks		

d-electrons concept [4]. The advantage of the use of this concept is to predict precisely the alloying limits of refractory elements in view of the phase stability even in high Cr superalloys [4].

It is generally accepted that the temperature capability decreases with increasing Cr content in the alloy [5]. But here to get the high corrosion resistance, 12%Cr superalloys are prepared by modifying the alloy composition of TUT92 [4], which is one of the highest performance 2nd generation nickel based superalloys developed by us previously. The Re content of TUT92 is 0.25mol% (0.75mass%), but there is no Re in the present 12%Cr superalloys.

Table 1 shows the chemical compositions of the six 12%Cr single crystal (SC) superalloys and one of the 2nd generation SC alloys containing 3%Re which is used as a reference alloy. In the table, the upper row and the lower row represent the alloy composition in mol% and in mass%, respectively. The compositional ratios of Ti/Al and Ta/(Mo+W) are varied in mol% units among these alloys.

$\overline{Md}$ and $\overline{Bo}$ values are also shown in the table. They are obtained from the compositional average of the d-electron parameters, Md and Bo [4,6]. Both $\overline{Md}$ and $\overline{Bo}$ are known to be related to the phase stability of nickel based superalloys. It is also known that high strength conventional nickel based superalloys including the 1st and the 2nd generation single crystal superalloys have special values, $\overline{Md}$: 0.975~0.995 and $\overline{Bo}$: 0.660~0.715 [4,7]. The $\overline{Md}$ and $\overline{Bo}$ values of the six alloys are set in these

ranges by adjusting the compositions of the refractory elements such as Mo, W and Ta in the alloys.

Alloy preparation and heat treatments

First, the master ingots of these alloys are made in a vacuum induction furnace by controlling the contents of gas elements to be as low as possible. Then, using those ingots, single crystals measuring 16mm in diameter and 150mm in length are grown by a directionally solidified method. The conditions of solution heat treatment and precipitation heat treatment of the γ ' phase are shown in Table 2. Every specimen is first heat treated following the conditions shown in Table 2 and then supplied for a series of experiments.

Microstructural observation

The microstructure of the SC alloys are observed with the SEM before and after the creep rupture tests. The cross section of the specimens after hot corrosion tests and oxidation tests are also observed using a SEM equipped with EDX analyzer. For these observations, the specimen surface is first polished mechanically with emery papers and then with buff together with water containing alumina powders. Subsequently, the surface is etched chemically in an HCl-HNO$_3$ solution.

Creep rupture test

The heat-treated SC alloys are machined mechanically into the specimens for the creep rupture test. The gauge length
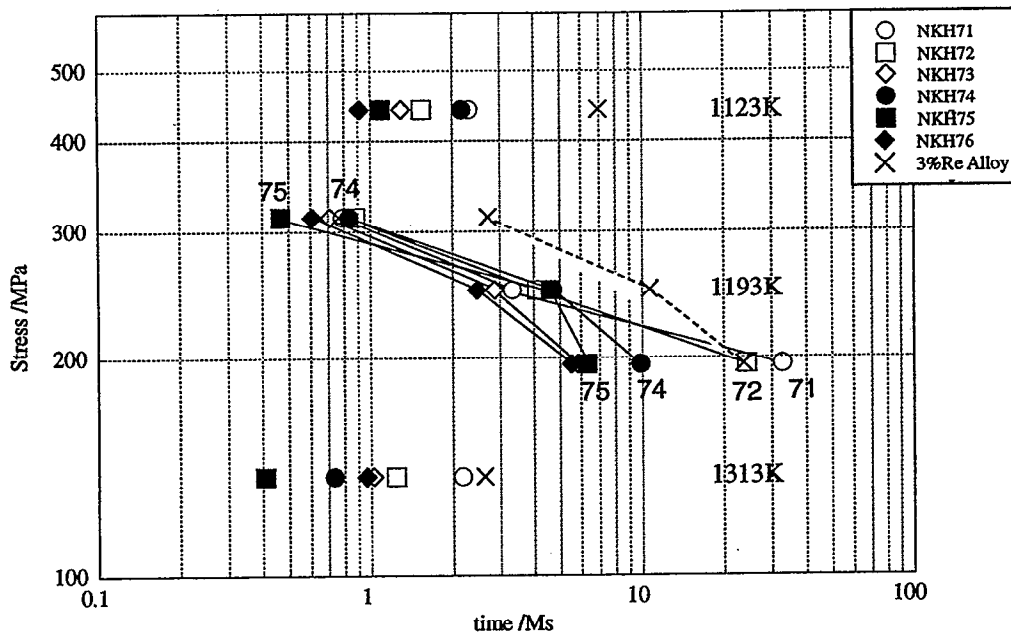
Fig.1 Results of creep rupture test.

of the specimen is 6mm in diameter and 30mm in length. The creep rupture tests are carried out under temperature/stress conditions of 1313K/137MPa, 1193K/314MPa, 248MPa, 196MPa, and 1123K/441MPa.

Oxidation and hot corrosion tests

The plate specimens measuring 10 x 25 x 1 mm are cut from the SC alloys by an electro-spark machine. Two kinds of oxidation tests are employed in this study. One is the cyclic oxidation test, in which the specimen is held in air at 1373K for 72ks followed by air cooling in each cycle. This cycle is repeated for 12 cycles, and the total exposure time at 1373K is 864ks. The other is the continuous oxidation test at 1313K for 2.16Ms.

In order to examine the hot corrosion resistance of the SC alloys, a burner-rig test is carried out at 1173K for 126ks with a specimen of 10mm in diameter and 30 mm in length. A fuel gas with atomized brine of 80ppm NaCl is used for this test. In addition, to prepare the specimens for the X-ray diffraction measurement, specimen surfaces of NKH71 and NKH76 are coated first with a solid solution of Na_2SO_4-25mol%NaCl salt, and then they are placed in a furnace at 1173K for 72ks.

Experimental Results

Creep strength

The results of the creep rupture test are shown in Fig.1. In the figure, the data on the reference alloy containing Re is

represented by a cross mark. As mentioned earlier, all the experimental alloys have similar $\overline{Md}$ and $\overline{Bo}$ values. In the range of these values, the measured creep rupture lives are dependent on the alloy compositions as follows;

(1) Mo+W content is an important factor for increasing the creep rupture life in all the test conditions. For example as shown in Table 1, NKH71 and NKH72 alloys, both containing the highest amount of Mo+W among the experimental alloys, show longer rupture lives than other experimental alloys.

(2) When comparing the result of NKH71 with that of NKH72, Co is supposed to be an effective element in improving the creep rupture life in the high stress levels at 1193K, but it does not work anymore in the low stress, 196MPa, at the same temperature.

NKH74 and NKH75 exhibit longer rupture lives under 248MPa at 1193K than NKH71 and NKH72. However, this is not the case under 196MPa at the same temperature. In particular, the creep rupture lives of NKH74 and NKH75 under 196MPa are much lower than the values extrapolated from the creep rupture data at the higher stress levels at 1193K. These results indicate clearly that the Larson-Miller plot is inapplicable to the present experimental alloys.

The metal temperature of the turbine blade is controlled to be below about 1200K by the thermal barrier coating (TBC) and by air cooling. Also, the stress level used for the plant design is not as high as 200MPa. Since the Larson-Miller plot does not apply here, an accelerating creep test by increasing temperature or stress will give us an erroneous
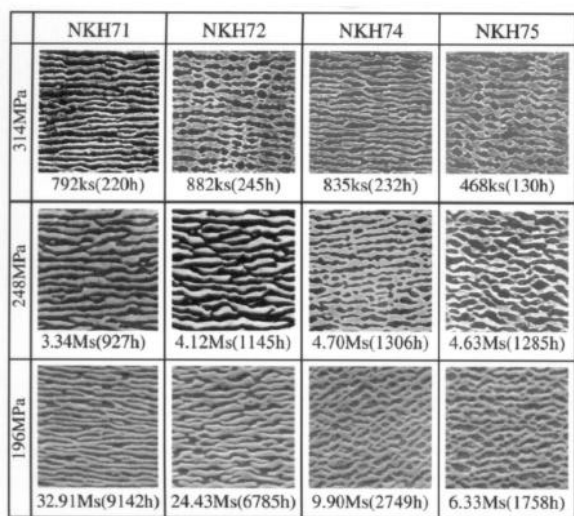
287

	NKH71	NKH72	NKH74	NKH75
314MPa	792ks(220h)	882ks(245h)	835ks(232h)	468ks(130h)
248MPa	3.34Ms(927h)	4.12Ms(1145h)	4.70Ms(1306h)	4.63Ms(1285h)
196MPa	32.91Ms(9142h)	24.43Ms(6785h)	9.90Ms(2749h)	6.33Ms(1758h)

Fig.2 Microstructures of the experimental alloys crept at 1193K under three stress levels.

Table 3 Aspect ratios of the γ' phase in the experimental superalloys crept at 1193K under three stress levels.

Alloy	Aspect ratio		
	314MPa	248MPa	196MPa
NKH71	49.2	34.5	21.9
NKH72	9.2	31.3	13.4
NKH74	50.0	14.1	5.9
NKH75	10.9	8.4	7.1
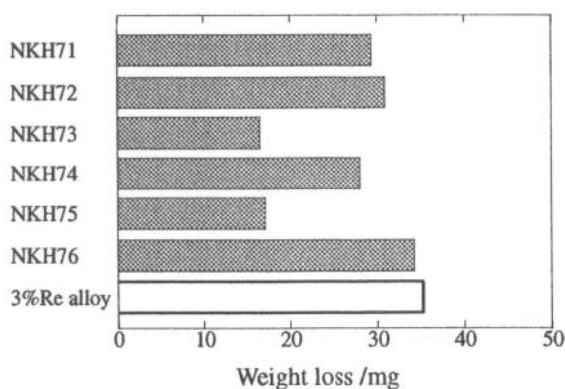
Weight loss /mg

Fig.3 Weight loss of specimens after cyclic oxidation.

answer as to the temperature capability of the alloy.

Rafted structure

The typical microstructures of NKH71, NKH72, NKH74 and NKH75 alloys crept at 1193K are shown in Fig.2. The rafted structure is observed in all the experimental alloys. The measured aspect ratios of the γ' phase obtained from the microstructures are listed in Table 3.

NKH71 and NKH72 alloys exhibit a regular rafted structure in all the stress conditions, whereas NKH74 and NKH75 alloys show somewhat irregular ones, except for NKH74 tested at 314MPa. These results imply that the coherency between the γ phase and the γ' phase is lost in both NKH74 and NKH75 alloys, in particular, in the case of low stress conditions (longer rupture life). This is related probably to the phenomena that the stress-time to rupture curve at 1193K becomes steep suddenly when the stress level is changed from 248MPa to 196MPa in these two alloys as shown in Fig.1.

Oxidation resistance

The results of the cyclic oxidation test are shown in Fig.3. The weight loss measured after 12 cycles is in the range of 17 to 35mg. The weight of the specimen decreases due to the peeling off or spalling of surface scales. All the experimental alloys are comparable or even superior in oxidation resistance when comparing to the reference alloy containing 3% Re. Among the experimental alloys, NKH73 and NKH75, show an indication of good oxidation resistance, in which the Ti/Al compositional ratio is about 0.33.

The microstructures are observed in the cross section of the oxidation surface. As shown in Fig.4, a layered structure is formed on the oxidation surface. The outermost layer consists of mainly Al oxide phase, and the middle layer contains Al nitride phase, and the inner layer contains Ti nitride phase. Some of these phases are identified as Al_2O_3, AlN and TiN by the EDX semi-quantitative chemical analysis. The reason why this layered structure is formed will be discussed later.

The results of the continuous oxidation test of the SC alloys tested at 1313K for 2.16Ms are shown in Fig.5, and are very different from the results of the cyclic oxidation test shown in Fig.3. The weight loss tends to increase approximately with the alloy number. However, no difference is seen in the oxidation products between the cyclic and the continuous oxidation tests. By comparing the results between NKH71 and NKH72, it is seen that Co is the element to deteriorate the oxidation resistance. Also, there is a trend that the resistance decreases with increasing Ti/Al compositional ratio, except for the 3%Re alloy.

Hot corrosion resistance

The results of the burner-rig test at 1173K for 126ks are shown in Fig.6. The weight loss decreases approximately with the alloy number. This implies that the hot corrosion resistance is improved by increasing the Ti/Al compositional ratio. This trend is opposite to the observation in the continuous oxidation test, as explained earlier. Furthermore, by comparing the results between NKH71 and NKH72, it is found that the Co addition improves the hot corrosion resistance considerably. This is also the reverse result of the continuous oxidation test.
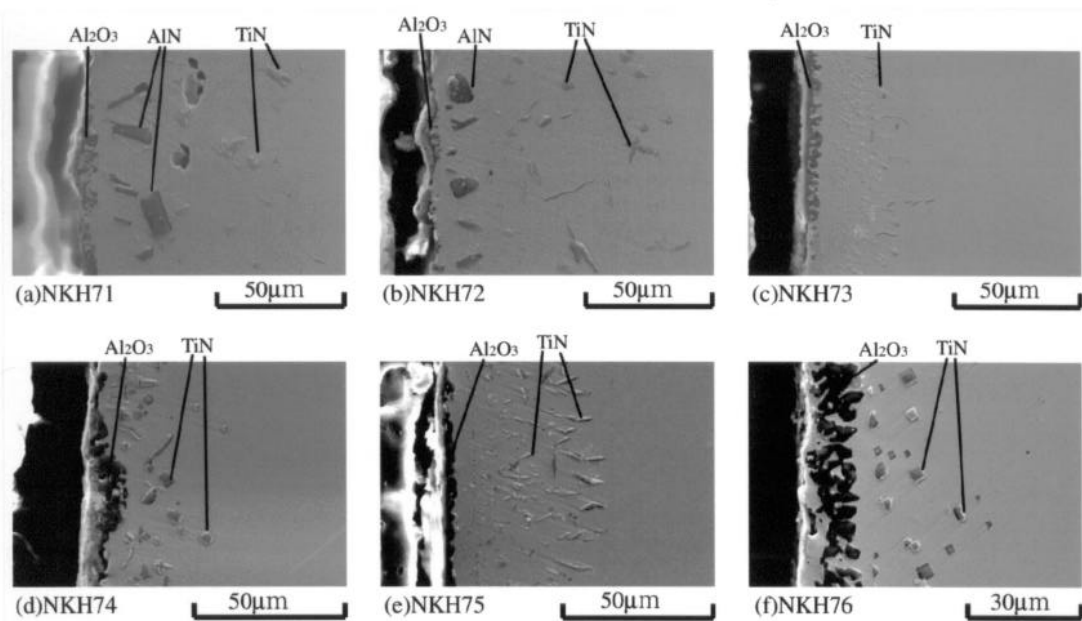
Fig.4   SEM microstructures in the cross section of specimens after the cyclic oxidation test.
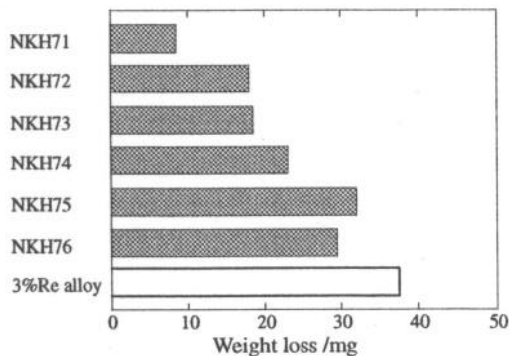

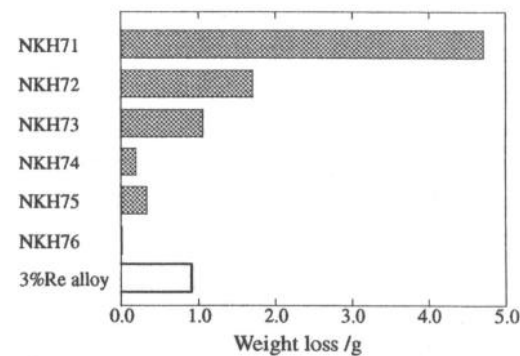Fig.5 Weight loss of specimens after continuous oxidation.

Fig.6 Weight loss of the specimens after the burner-rig test.

Among the experimental single crystal superalloys, the hot corrosion resistance is best for NKH76 and worst for NKH71. The main compositional differences between NKH71 and NKH76 are in Al, Ti and W contents.   In other words, high Ti/Al compositional ratio and low W content are conducive to better hot corrosion resistance in the alloys. Interestingly, in spite of a relatively high Cr content, 12mass%, in all the experimental alloys, the hot corrosion resistance is quite different among them.   This clearly indicates that the addition of 12mass%Cr is not necessarily needed to get good hot corrosion resistance.

After the burner-rig test, the SEM micrographs and the corresponding characteristic X-ray images are taken from a cross section of NKH71 and NKH76 alloys, and the results are shown in Fig.7 and Fig.8, respectively.   Schematic illustration is also drawn in each figure to show the layered structure of corrosion products.   Needless to say, the thickness of the corrosion layer is directly related to the weight loss shown in Fig.6, and is about 130 μm in NKH71

and about 30 μm in NKH76.   By comparing Fig.7 with Fig.8, it is apparent that the appearance of the layered structure formed in the corrosion surface resembles, for example, the sulfide layer existing beneath the oxide layer in both cases.   This is consistent with the previous result [8].   However, there is still a large difference between NKH71 and NKH76 in the state of the TiO_2 layer.   Namely, TiO_2 formed on the outermost surface is dense in NKH76 (Fig.8) but porous in NKH71 (Fig.7).   Furthermore, Cr sulfide is observed clearly in the corrosion products of NKH71, resulting in the existence of Cr depleted regions in this alloy.

The results of X-ray diffraction are shown in Fig.9 for (a) NKH71 and (b) NKH76, both measured after the hot corrosion test.   As described above, the main difference in the layered structure between NKH71 and NKH76 is whether a TiO_2–rich layer exists or not in the surface layer.   In fact, as shown in Fig.9 (b), TiO_2 is observed on the outer surface of good corrosion resistant NKH76.   However, as shown in
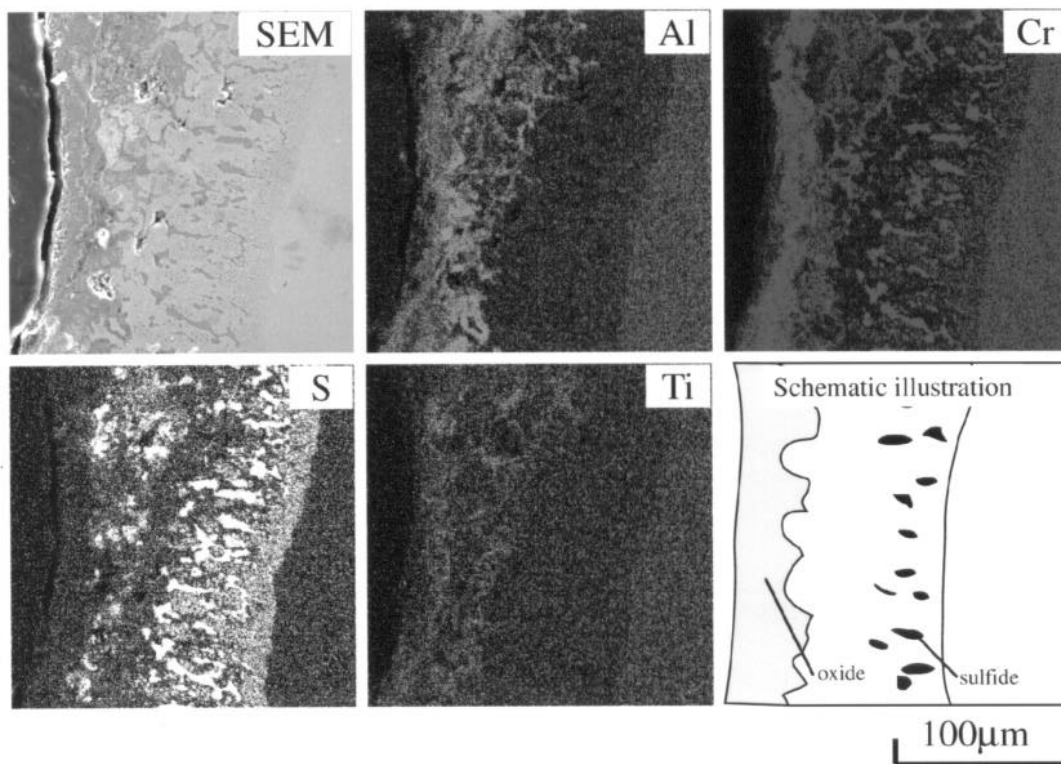
Fig.7   SEM image and the corresponding characteristic X-ray images taken from a cross section of NKH71 after the burner-rig test.

Fig.9 (b), it is not detectable clearly on the surface of poor corrosion resistant NKH71.

Discussion

Creep strength

It is well known that the γ' phase in nickel based superalloys changes its shape from cuboidal to rafted structure during the high temperature creep [9]. The mechanism of this phenomenon has been studied theoretically since the 1970's [10-12], and it is understood that both the lattice misfit and the elastic constant difference between the γ phase and the γ' phase play an important role in the formation of the rafted structure [13]. As long as the coherency between the two phases is maintained, the elastic constant difference between them will operate to form such a rafted structure [11, 13].

NKH71 appears to keep the coherency between the γ phase and the γ' phase up to about 33Ms at 1193K. This is because, once the coherency is lost in the alloy, the γ' phase tends to coagulate and show an irregular microstructure, in order to lower the interfacial (chemical) energy by reducing the interfacial area in unit volume. In the case of NKH71, this never happens even after 33Ms, as shown in Fig.2.

On the other hand, the rafted structures in NKH74 and NKH75 are more irregular when compared to those in NKH71 and NKH72, despite the same creep conditions (1193K/196MPa) employed in these alloys. Therefore, it is supposed that there is a larger lattice misfit in NKH74 and NKH75 than in NKH71 and NKH72. As a result, the coherency between the γ and γ' phases in NKH74 or NKH75 is lost considerably and misfit dislocations are introduced into the interface. The existence of such dislocations at the interface lowers the elastic energy between the two phases, so that the interfacial energy effect becomes more dominant than the elastic energy effect. As a result, the shape of the γ' phase becomes round and irregular. In fact, the lattice mismatch of the NKH74 alloy is estimated to be 0.56% by using a relationship between the lattice constants and the chemical composition [14,15]. This lattice mismatch, 0.56%, for NKH74 is much larger than 0.38% for NKH71 and 0.35% for NKH72.

The relationship between the rafted structure and the creep strength depends on the creep temperature and the stress level as well. It is said that when dislocations do not cut the γ' phase, the rafted structure gives a long way for dislocation climbing, resulting in the improvement of the creep rupture strength, but otherwise the creep strength tends to decrease by the rafting of the γ' phase in the alloy [13].

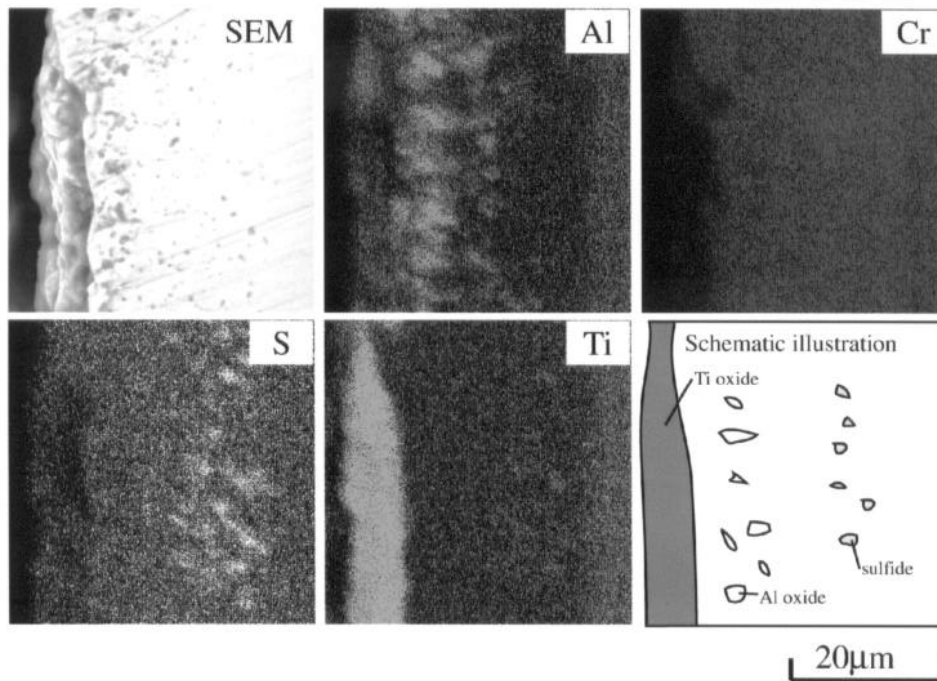#### Deviation from Larson-Miller plot

Fig. 8   SEM image and the corresponding characteristic X-ray images taken from a cross section of NKH76 after the burner-rig test.
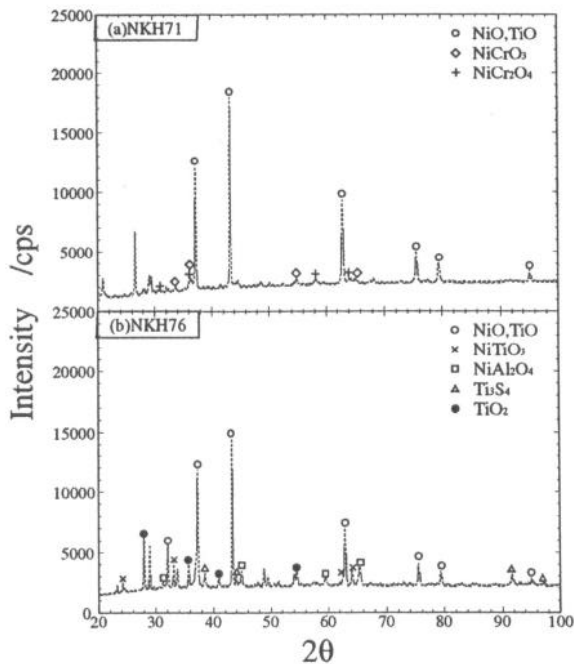

Fig. 9   X-ray diffraction patterns of (a) NKH71 and (b) NKH76 after the hot corrosion test using the coating method.

It is stressed here that creep rupture data obtained at 1313K/137MPa are not usable for predicting the creep rupture life at 1193K/196MPa, by using a conventional Larson-Miller parameter.   For example, Fig.10 is a Larson-Miller plot (C=30) which is drawn by using the creep data shown in Fig.1.   In general, the Larson-Miller plot shows a smooth curve, when the microstructure in the alloy does not change during creep.   However, as shown in Fig.10, the plot appears to give two different lines as indicated by A and B.   Line A is obtained at high stress levels, whereas line B is obtained at low stress levels.   It is likely that these two lines, A and B, are concerned with microstructural change during creep.   In particular, the discrepancy between the A part and the B part in Fig.10 is larger in NKH74 and NKH75 than in NKH71 and NKH72. This is consistent with the results that the microstructures both of NKH71 and NKH72 are more stable during creep than those of NKH74 and NKH75, as shown in Fig.2.

Here, the data obtained at 1193K is located in the transition region from A to B.   As mentioned before, the temperature, 1193K, corresponds to the upper limit temperature for the turbine blades to be serviced for a long term in industrial gas turbines.   Also, stress operating on the turbine blades during the current service of gas turbines is not as high as 200MPa.   Since the Larson-Miller plot is no longer valid in this temperature and stress range, creep experiments around 1193K/196MPa are important for testing the temperature capability of nickel based superalloys used in industrial gas turbines.
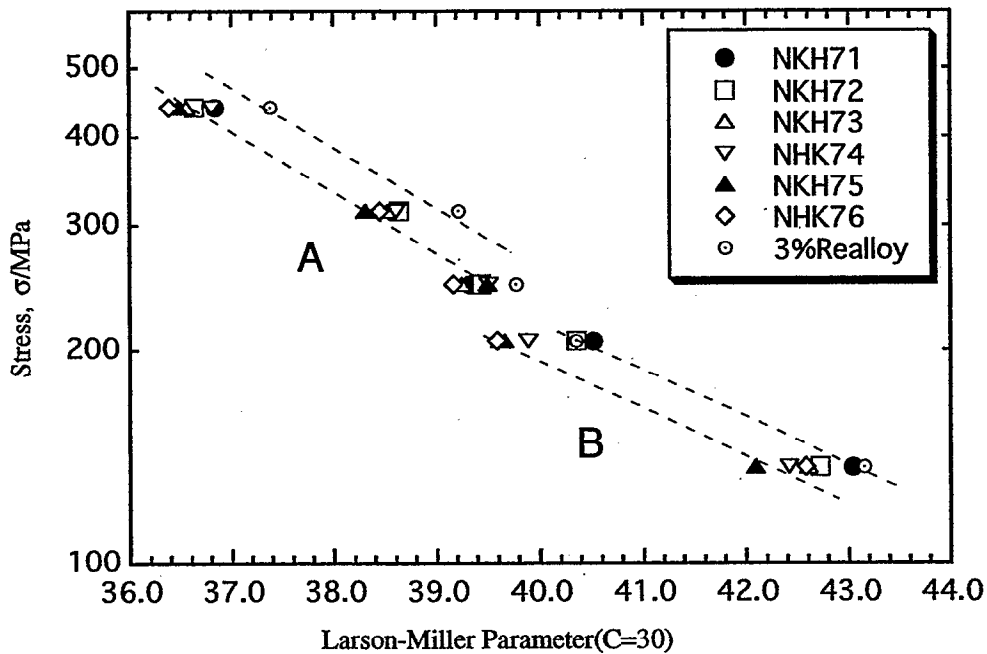
Fig. 10 Larson-Miller plot of the creep rupture data

Oxidation resistance and hot corrosion resistance

Both oxidation and hot corrosion resistance are important for materials used for blades and vanes in industrial gas turbines. In general, Al is known to be an effective element in improving high temperature oxidation resistance. Also, Cr is believed to be an effective element in improving hot corrosion resistance. However, in spite of the same Cr content, the hot corrosion resistance is considerably different among the present six experimental SC alloys. For example, the weight change is about two orders of magnitude larger in NKH71 than in NKH76.
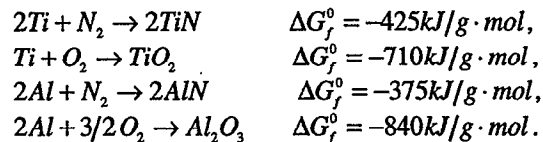
In Fig. 11 the results are plotted of both the burner-rig test and the continuous oxidation test. From this figure, it is clearly determined that the alloying effect is very different between the hot corrosion resistance and the oxidation resistance. As mentioned earlier, the increase in Ti/Al compositional ratio deteriorates the oxidation resistance but improves the hot corrosion resistance.

Possible mechanism for oxidation

In order to improve the oxidation resistance, it is necessary to form a dense oxide layer on the specimen surface. Both Ti and Al are strong oxide forming elements, so the oxidation occurs in a competitive way. It is known that the competitive reaction impedes the formation of a dense oxide layer [16]. Therefore, a purely dense oxide layer can not be formed on the specimen surface as long as the alloy contains comparable amounts of Al and Ti. Also, it is

considered that nitrides play an important role in the oxidation resistance, because nitrides are formed under the oxide layer in the oxidized specimen (see Fig.4). As explained below, this nitridation probably plays a role in the oxidation resistance in a similar way that the sulfidation does in the hot corrosion resistance.

The standard free energies of formation for TiN, TiO_2, AlN and Al_2O_3 are given as follows [17]:

$$2Ti + N_2 \rightarrow 2TiN \qquad \Delta G_f^0 = -425 kJ/g \cdot mol,$$
$$Ti + O_2 \rightarrow TiO_2 \qquad \Delta G_f^0 = -710 kJ/g \cdot mol,$$
$$2Al + N_2 \rightarrow 2AlN \qquad \Delta G_f^0 = -375 kJ/g \cdot mol,$$
$$2Al + 3/2 O_2 \rightarrow Al_2O_3 \qquad \Delta G_f^0 = -840 kJ/g \cdot mol.$$

At the beginning of oxidation in air, both oxides and nitrides are most likely to be formed. However, since oxides are more stable than nitrides, nitrides will be oxidized if the oxygen activity is higher than a certain level. For example, AlN is also one of the most stable nitrides, but still it is more unstable than Al_2O_3, judging from the standard free energy of formation. So, even if AlN is formed on the specimen surface, it turns to Al_2O_3 easily.

If a dense Al_2O_3 layer is formed predominantly on the specimen surface, the oxidation rate of the alloy will decrease greatly. This is plausible in those alloys (e.g., NKH71) which contain a high Al content. Following the above discussion, it will be necessary to hold free nitrogen

292

released by the oxidation of AlN. A small amount of Ti may be enough to capture such nitrogen, because TiN is relatively stable and it may be hard to change TiN into TiO_2. In fact, as shown in Fig.12, fine TiN precipitates are observed under the Al_2O_3 layer of NKH71 after the continuous oxidation test. Similarly, NKH73 and NKH75, both exhibiting a good indication of the cyclic oxidation resistance, have a dense Al_2O_3 layer and fine TiN precipitates under the layer, as shown in Fig.4

On the other hand, in the relatively Ti-rich alloys, TiN will form together with TiO_2 at the beginning of oxidation. But this TiN may not be oxidized to form TiO_2 so readily, judging from the small standard free energy difference between TiN and TiO_2. Therefore, the condensed TiO_2 layer may not be formed in the presence of TiN and Al_2O_3 in such alloys, resulting in poor oxidation resistance. Needless to say, if the Ti content is comparable to the Al content, the alloy can no longer form either dense Al_2O_3 nor TiO_2 as explained above. Thus, the Ti/Al compositional ratio influences the oxidation resistance greatly.

The oxidation mechanism mentioned here will be approximately correct, but there is a difference in the results between the cyclic and the continuous oxidation tests (Fig.3 and Fig.5). This is probably because the factor of adherence of the oxide layer to the specimen surface is more important in the cyclic oxidation than in the continuous oxidation. In other words, the thermodynamic consideration mentioned here is not applicable simply to the cyclic oxidation because of its dynamical phenomenon.

Possible mechanism for hot corrosion

As previously explained above, there is a large difference in the weight loss obtained from the burner-rig test among the alloys, despite their similar Cr content in them. It is well known that the addition of W and Mo deteriorates the hot corrosion resistance of nickel based superalloys by the acidic fluxing reaction [18]. NKH71 and NKH72 have a higher level of W and Mo content than the other experimental alloys. So, this is one of the reasons why these two alloys show poor hot corrosion resistance. By comparing the result of the hot corrosion between NKH71 and NKH72, it is seen that the Co addition improves the resistance, but the mechanism is still not clear at the moment. Also, as is evident from Table 1 and Fig.6, the compositional ratio, Ta/(W+Mo), needs to be set at about unity to increase the resistance, which is consistent with our previous result [4].

In the cross section of the specimen surface observed after the burner-rig test, a sulfide layer is present beneath the oxide layer. In general, it is known that sulfidation occurs prior to oxidation, and then sulfides are oxidized. Such sulfidation and subsequent oxidation reactions take place alternately and repeatedly, and the two layers penetrate into the base metal deeply. Therefore, the hot corrosion resistance will be improved if the sulfidation reaction is suppressed in some way. In NKH76, which shows the best hot corrosion resistance among the present experimental
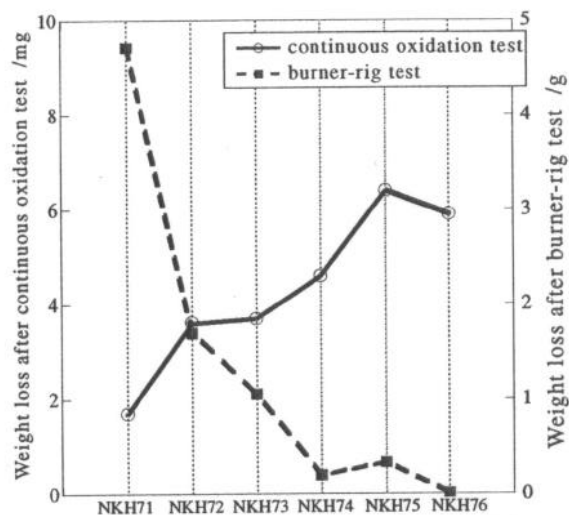

Fig.11 Comparison in the weight loss of the specimens between the continuous oxidation test and burner-rig test.
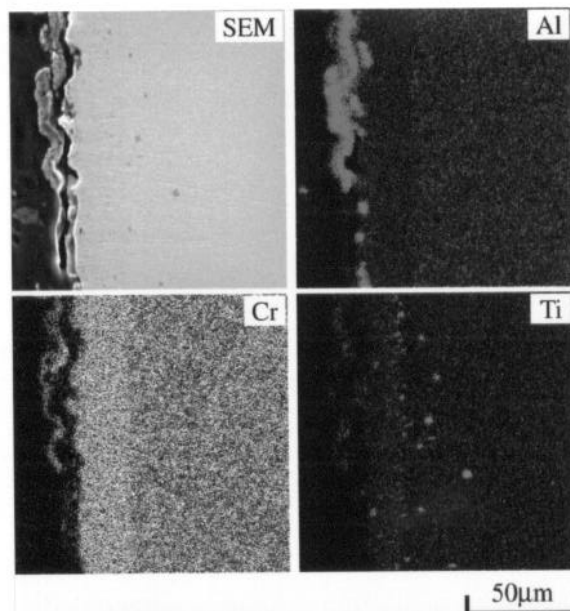

Fig.12 SEM image and the corresponding characteristic X-ray images taken from the cross section of NKH71 after the continuous oxidation test.

alloys, the dense TiO_2–rich layer is observed in the outermost layer of the corrosion products, as shown in Fig.8. From this result, it is deduced that the dense TiO_2–rich layer forms so quickly on the specimen surface when the alloy contains a certain level of Ti content because of the higher stability of TiO_2 than Cr_2O_3. In such a case, Cr is never oxidized in the presence of TiO_2 because of its higher dissociation pressure than TiO_2, but instead Cr can hold sulfur and form a sulfide under the oxide layer. As a result, sulfidation does not proceed into the base metal any longer, resulting in the maintenance of good hot corrosion resistance in NKH76.

Conclusion

In order to develop high performance nickel based superalloys for industrial gas turbines, 12mass% (14mol%)Cr and no Re alloys are made with the aid of the d-electrons concept, and the alloying effects are examined on the creep rupture strength, oxidation resistance and hot corrosion resistance. Among the experimental alloys, NKH71 exhibits the longest creep rupture life, 32.9Ms (9142h), at 1193K under a stress of 196MPa. NKH71 is superior in creep strength to the 2nd generation SC superalloy containing 3%Re. Also, it is shown that the Larson Miller plot is not suitable for presumption of longer rupture life in nickel based superalloys. In addition, the optimization of Ti/Al compositional ratio is found to be most important in improving both hot corrosion resistance and oxidation resistance at high temperatures. The amount of 12mass%Cr is not needed to get good hot corrosion resistance, as long as both the compositional ratios of Ti/Al and Ta/(W+Mo) are high in the alloy.

Acknowledgement

References

[1] R.Kehlhofer, "Power Engineering-Status and Trends", Materials for Advanced Power Engineering 1998, Eds. J. Lecomte-Beckers, et al., Forchungszentrum, Jülich, 1998, pp.3-17.

[2] W. S. Walston et al., "Rene N6: Third Generation Single Crystal Superalloy", Superalloys 1996, Eds. R.D. Kissinger et al., TMS, Warrendale, 1996, pp.27-34.

[3] G.L.Erickson, "The Development and Application of CMSX-10", ditto, pp.35-44.

[4] K. Matsugi et al. "Realistic Advancement for Nickel-Based Single Crystal Superalloys by the d-Electrons Concept", Superalloys 1992, Eds. S.D. Antolovich et al, TMS, Warrendale, pp. 307-316.

[5] R.F. Singer, "Advanced Materials and Processes for Land-Based Gas Turbines", Materials for Advanced Power Engineering 1994, Eds. D. Coutsouradis et al, Kulwer Academic Publishers, Dordrecht, 1994, pp. 1707-1730.

[6] M.Morinaga et al., "New PHACOMP and its Application to Alloy Design", Superalloys 1984, Eds. M.Gell et al, The Metall. Soc. Of AIME, (1984), pp.523-532.

[7] Y. Murata, M.Morinaga and R. Hashizume, "Trace of the Evolution of Ni-Based Superalloys by the d-Electrons Concept", Materials for Advanced Power Engineering 1998, Eds. J. Lecomte-Beckers, et al., Forchungszentrum, Jülich, 1998, pp. 1381-1390.

[8] G.Y. Lai, High Temperature Corrosion of Engineering Alloys, (Metals Park OH, ASM International, 1990), pp.117-144.

[9] J.K. Tien and S. M. Copley, "The Effect of Uniaxial Stress on the Periodic Morphology of Coherent Gamma Prime Precipitatate in Nickel-Base Superalloy Crystals", Metall. Trans., 2 (1971), pp.217-219.

[10] A. Pineau, "Influence of Uniaxial Stress on the Morphology of Coherent Precipitates suring Coarsening-Elastic Energy Considerations", Acta Metall., 24 (1976), pp.559-564.

[11] T. Miyazaki, K. Nakamura and H. Mori, "Experimental and Theoretical Investigations on Morphological Changes of γ' Precipitates in Ni-Al Single Crystals During Uniaxial Stress-annealing", J. Mater. Sci., 14(1979), pp.1827-1837.

[12] S. Socrate and D. M. Parks, "Numerical Determination of the Elastic Driving Force for Directional Coarsening in Ni-Superalloys", Acta Metall., 41 (1993), pp.2185-2209.

[13] F. R. N. Nabbaro, "Rafting in Superalloys", Metall. Mater. Trans. A, 27A (1996), pp.513-530.

[14] H. Harada and M. Yamazaki, "Alloy Design for γ' Precipitation Hardening Nickel-base Superalloys Containing Ti, Ta, and W", Tesu-to-Hagane, 65 (1979), pp.1059-1068.

[15] Y. Murata, S. Miyazaki and M. Morinaga, "Evaluation of the Partitioning Ratios of Alloying Elements in Nickel-Based Superalloys by the d-Electrons Parameters", Materials for Advanced Power Engineering 1994, Eds. D. Coutsouradis et al, Kulwer Academic Publishers, Dordrecht, 1994, pp. 909-918.

[16] Y. Murata et al., "Early Stage of High Temperature Oxidation of TiAl and FeAl at Low Oxygen Partial Pressures", J.Japan Inst. of Metals, 61 (1997), pp.702-709.

[17] S. Nagasaki ed.,"Metals Databook, 2nd ed.", Japan Inst. Met., 1983, pp.90-91.

[18] F.S. Pettit and G.H. Meier, "Oxidation and Hot Corrosion of Superalloys", Superalloys 1984, Eds. M.Gell et al, The Metall. Soc. Of AIME, (1984), pp.651-687.